HALITE AND SPHALERITE IN THE SIDI EL HABIB 001 (H5) ORDINARY CHONDRITE: INSIGHTS INTO MICROCHEMISTRY-CONTROLLED HYDROTHEMAL ALTERATION ON ITS PARENT BODY.

S. Che[1], K. J. Domanik[1], and T. J. Zega[1,2], [1]Lunar and Planetary Laboratory, University of Arizona, Tucson AZ, [2]Department of Materials Science and Engineering, University of Arizona, Tucson AZ. (sche@arizona.edu)

Introduction: Recent petrologic and mineralogic studies of type 4-6 ordinary chondrites (OCs) provide strong evidence for the presence of fluids during advanced thermal metamorphism on their parent asteroids [1–3], challenging the conventional view that equilibrated OCs experienced metamorphism under dry conditions [4]. The newly discovered H5 OC Sidi El Habib 001 (SEH 001) contains abundant halite which replaces albitic plagioclase and chlorapatite, providing new insights into the hydrothermal alteration processes of OCs [5]. SEH 001 is the third halite-bearing OC sample recognized, besides Monahans (1998) and Zag [6,7]. Here we report observations of halite and associated phases in SEH 001 that reveal sub-micron alteration features. We also report preliminary data on sphalerite in this sample which was first discovered by [8], and as we will show, it is an important probe of the fluid compositions in the alteration history of SEH 001.

Sample and Methods: A one-inch round polished-thick section (#2169_C4) of SEH 001 was loaned to us from the Buseck Center for Meteorite Studies at Arizona State University. We acquired wavelength dispersive X-ray spectroscopy (WDS) maps on a Cameca SX-100 electron probe microanalyzer (EPMA) located in the Kuiper Materials Imaging and Characterization Facility (KMICF) at the Lunar and Planetary Laboratory (LPL), University of Arizona. More detailed information on sample microstructure was acquired with a Hitachi S-4800 scanning electron microscope (SEM) equipped with energy-dispersive X-ray spectrometry (EDS). Multiple focused-ion-beam (FIB) sections were prepared using a Thermo Scientific Helios NanoLab 660 G^3 FIB-SEM in KMICF. The characterization work of the FIB sections was conducted on the 200 keV Hitachi HF5000 scanning transmission electron microscope (S/TEM) in KMICF.

Results: Halite in the FIB sections is very sensitive to laboratory moisture and can quickly deliquesce and evaporate, even in an N_2-filled desiccator. Therefore, all the FIB sections were examined in the TEM immediately after the preparation.

TEM observations of halite and associated phases. Two FIB sections were extracted from interfacial regions between halite and plagioclase in SEH 001. The STEM images and EDS maps reveal that plagioclase is extensively replaced by halite, with relict grains (a few hundred nm) of plagioclase (~$Ab_{77.2}Or_{8.8}$), a lesser amount of olivine (~$Fo_{81.5}$), and pyroxene (~$En_{82.3}Wo_{1.8}$) partly or completely enclosed within halite and its terrestrial weathering product (compositionally similar to akaganéite, β-FeO(OH,Cl)) (Fig. 1). Some pyroxene grains also occur as fine-grained aggregates in one of the FIB sections.

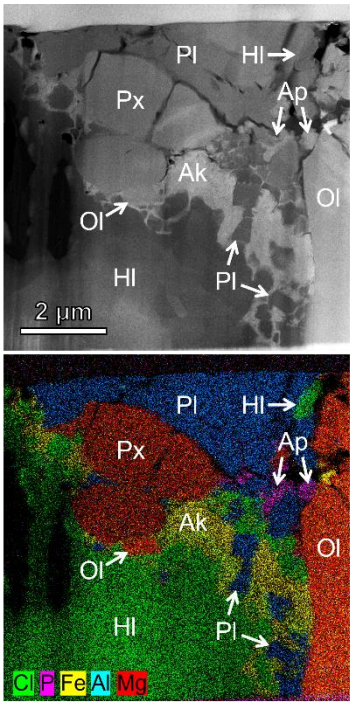

Fig. 1. Dark-field STEM image and combined EDS map of a FIB section that transects the plagioclase-halite interface. Plagioclase is partially replaced by halite, with relict plagioclase inclusions in halite and akaganéite. Abbreviations: Ak, akaganéite; Ap, apatite; Hl, halite; Ol, olivine; Pl, plagioclase; Px, pyroxene.

We also lifted out two FIB sections from the regions where chlorapatite is replaced by halite. From the TEM observations, some halite grains occur in the interstitial regions between chlorapatite and coarse-grained olivine, and have corroded interfaces with chlorapatite. A coarse-grained halite (single crystal as confirmed by electron-diffraction patterns) in one of the FIB sections has an akaganéite weathering layer that contains a relict plagioclase grain (~750 nm), suggesting that plagioclase is also being replaced by halite in these regions.

An additional two FIB sections were prepared from the periphery of two chondrules where plagioclase mesostasis contacts the matrix to investigate potential alteration features related to the halite formation in the matrix. From the backscattered electron (BSE) images, the plagioclase mesostasis of both chondrules is highly porous, relative to the matrix, and contains abundant fine-grained inclusions of chromite and ilmenite (typically <1 μm). The STEM EDS analyses show that the plagioclase mesostasis only contains ≤0.3 wt% Cl

and no Cl-bearing phases were identified within plagioclase. Pores and fractures in the FIB sections contain elevated Cl concentrations of ≤3.2 wt%.

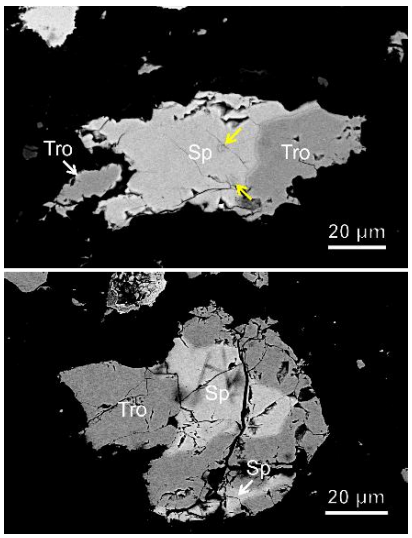

Fig. 2. BSE images of representative intergrowths of sphalerite and troilite. Inclusions of troilite can occur in sphalerite (yellow arrows). Abbreviations: Sp, sphalerite; Tro, troilite.

Sphalerite and associated phases. Our previous report on the thick section of SEH 001 [5] showed that it is composed of a halite-free lithology embedded in a halite-bearing lithology. The two lithologies have very similar textures and mineralogy with otherwise obscure boundaries that are most easily recognized in the Cl X-ray maps. WDS mapping on the section reveals ubiquitous sphalerite only in the halite-bearing lithology. The size of sphalerite varies from several tens of μm to >100 μm. Sphalerite commonly intergrows with troilite (Fig. 2) and can contain inclusions of troilite, plagioclase, olivine, and pyroxene. The average EDS compositions of sphalerite give an empirical formula of $(Fe_{0.4}Zn_{0.6})S$, based on two atoms per formula unit. The coexisting troilite grains do not contain detectable Zn. Chromite (typically 10-20 μm in diameter) that occurs near sphalerite contains elevated Zn concentrations (~2.7 wt% on average) and minor Mg (~0.58 wt%), Al (~1.45 wt%), and Ti (~1.76 wt%).

Discussion: The clear textural evidence for halite replacing albitic plagioclase and chlorapatite in SEH 001 suggests that halite in this sample formed by hydrothermal alteration. Compared with hydrous minerals (such as phyllosilicates), halite is thermally more stable and could survive high metamorphic temperatures [9,10]. That halite replaces plagioclase and apatite suggests that it formed during advanced thermal metamorphism on its parent body. We note however, that in-situ formation of halite in SEH 001 contrasts with the exogeneous origin of halite proposed for Monahans (1998) and Zag [6,11], suggesting that halite can form through multiple chemical pathways.

Beyond akageneite, which is a terrestrial alteration product, the EPMA and TEM data suggest that the halite-bearing and halite-free lithologies were likely affected by fluids with different Cl concentrations. A possible explanation for different fluid compositions in SEH is the heterogeneous distribution of HCl hydrate ($HCl{\cdot}3H_2O$) that condensed from the solar nebular gas [12]. Additionally, the absence of halite in chondrules from the halite-bearing lithology points to micron-scale variations in fluid chemistry. Based on work by [13], we hypothesize that the fluid pH in chondrules and surrounding matrix likely differed due to their different total surface areas. Such a pH difference could have resulted in a more favorable condition for precipitation of albitic plagioclase in the matrix [14]. The preferential precipitation of plagioclase in the matrix is consistent with the much lower porosity of matrix plagioclase in SEH 001. Presumably, the higher Na activity in the matrix resulted in preferential formation of halite.

Sphalerite provides an additional line of evidence for varied fluid compositions on the parent body of SEH 001. High Cl contents and low pH in an aqueous fluid can significantly enhance the solubility of Zn via formation of Zn-Cl complexes [15]. Therefore, we hypothesize that Zn was dissolved into the initial Cl-rich fluid with low pH and later precipitated as sphalerite when pH became more basic. This hydrothermal alteration scenario can explain the presence of sphalerite only in the halite-bearing lithology.

Acknowledgments: We thank Dr. Laurence Garvie for preparation and loan of the section, and bringing sphalerite to our attention. This research was supported by the NASA grant #80NSSC19K0509.

References: [1] Kovach H. A. and Jones R. H. (2010) *Meteorit. Planet. Sci.*, *45*, 246–264. [2] Lewis J. A. et al. (2022) *Geochim. Cosmochim. Acta*, *316*, 201–229. [3] Jones R. H. et al. (2016) *Am. Mineral.*, *101*, 2452–2467. [4] Brearley A. J. and Krot A. N. in *Metasomatism Chem. Transform. rock*, Springer, Berlin Heidelberg, 2013, *56*, 659–789. [5] Che S. and Zega T. J. (2022) *Annu. Meet. Meteorit. Soc.*, *85*, #6012. [6] Zolensky M. E. et al. (1999) *Science*, *285*, 1377–1379. [7] Rubin A. E. et al. (2002) *Meteorit. Planet. Sci.*, *37*, 125–141. [8] Garvie, L. A. J. (2021) *Meteoritical Bulletin Database*. [9] Almeida K. M. F. and Jenkins D. M. (2017) *Am. Mineral.*, *102*, 2484–2493. [10] Bakker R. J. (2012) *Mineral. Petrol.*, *105*, 1–29. [11] Chan Q. H. S. et al. (2018) *Sci. Adv.*, *4*. [12] Zolotov M. Y. and Mironenko M. V. (2007) *Lunar Planet. Sci.*, *38*, #2340. [13] Brearley A. J. (2006) *Lunar Planet. Sci.*, *37*, #2074. [14] Dobrică E. and Brearley A. J. (2014) *Meteorit. Planet. Sci.*, *49*, 1323–1349. [14] Xing Y. et al. (2022) *Geochim. Cosmochim. Acta*, *330*, 131–147.